ELSEVIER

PII: S0032-3861(96)01039-7

Polymer Vol. 38 No. 17, pp. 4433–4438, 1997
© 1997 Elsevier Science Ltd
Printed in Great Britain. All rights reserved
0032-3861/97/$17.00+0.00

Phase separation behaviour in blends of isotactic polypropylene and ethylene–propylene diene terpolymer

C.-Y. Chen, W. Md. Z. W. Yunus*, H.-W. Chiu and T. Kyu†
Institute of Polymer Engineering, The University of Akron, Akron, OH 44325, USA
(Received 13 September 1996; revised 30 October 1996)

Miscibility and phase separation behaviour in blends of isotactic polypropylene (iPP) and ethylene–propylene diene terpolymer (EPDM, ethylene content 70%) have been examined by means of depolarized light scattering, polarizing optical microscopy, differential scanning calorimetry and dynamic mechanical methods. A cloud point phase diagram was established by means of light scattering after eliminating the influence of iPP crystal melting on liquid–liquid phase separation of iPP/EPDM blends. A lower critical solution temperature (LCST) was observed above the crystallization temperature, but below the melting temperature of iPP. This LCST is thermally reversible, so long as crystallization does not occur in its vicinity. The coupling between the crystal melting and liquid–liquid phase separation has been examined. Crystallization-induced phase separation and morphology development during crystallization of iPP have been investigated. © 1997 Elsevier Science Ltd.

(Keywords: iPP/EPDM blends; phase separation; LCST; crystallization; spinodal decomposition)

INTRODUCTION

In recent years, liquid–liquid phase separation in binary amorphous polymer blends has advanced remarkably in both theoretical and experimental aspects, whereas the progress is less significant in the miscibility studies of two-crystalline polymer blends, particularly the determination of phase diagrams involving crystal melting transitions[1–8]. The primary reason for this limited success is the influence of melting/crystallization of the crystalline component on phase separation behaviour and the resulting morphologies of the blends[3–8]. When the problem of crystal ordering transitions is imposed on the phase separation phenomena, one can appreciate the profound effect of crystallization on the equilibrium phase diagram, as well as on non-equilibrium pattern formation.

Recently, the competition between the crystal transition and phase separation in binary crystalline polymer blends has become an interesting issue in the field of polymer blends[3–10] and therefore is of interest to us. The melt blends of isotactic polypropylene (iPP) with ethylene–propylene diene terpolymer (EPDM) have been perceived to be completely immiscible[11–15]. While melt blending has been a favoured industrial practice, the poor mixing in a given processing equipment in conjunction with contamination can lead to erroneous conclusions, in particular when the system is marginally miscible or thermally unstable. Because of the strong perception of the reported immiscible character of the iPP/EPDM melt blends[11–15], there has been little or no effort towards investigation of the miscibility of the iPP/EPDM blends prepared by solution mixing.

In the present paper, miscibility phase diagrams of solvent mixed iPP/EPDM blends have been established by first eliminating the influence of crystal melting using laser light scattering. The morphology development driven by the liquid–liquid phase separation has been studied by depolarized light scattering and optical microscopy. The development of blend morphology resulting from the competition between crystallization and liquid–liquid phase separation has been investigated.

EXPERIMENTAL

iPP having an average molecular weight (M_w) of 247 000 was purchased from Scientific Polymer Products, Inc. EPDM having a moderate level of diene content, i.e., about 5% of ethylene norbornene (ENB), and ethylene content of 70% by weight of the copolymer was kindly supplied by Exxon Chemical Co. The Mooney viscosity of the EPDM was 55. Various blends of iPP/EPDM were prepared by first dissolving iPP powders in xylene at 130°C, then EPDM was added after lowering the temperature to 100°C and stirred thoroughly for about 90 min to ensure complete mixing. Film specimens were prepared by solvent casting at ambient temperature in a fume hood and dried in a vacuum oven at room temperature for 48 h. The thickness of the blend films used for light scattering and optical microscopy was approximately 10–20 μm. Flake samples were also prepared by pouring the solution into a non-solvent such as ethanol and washed for several times and dried at ambient temperature. The flakes were further dried in a

* Present address: Department of Chemistry, Universiti Pertanian Malaysia, 43400 UPM, Serdang Selangor, Malaysia
† To whom correspondence should be addressed

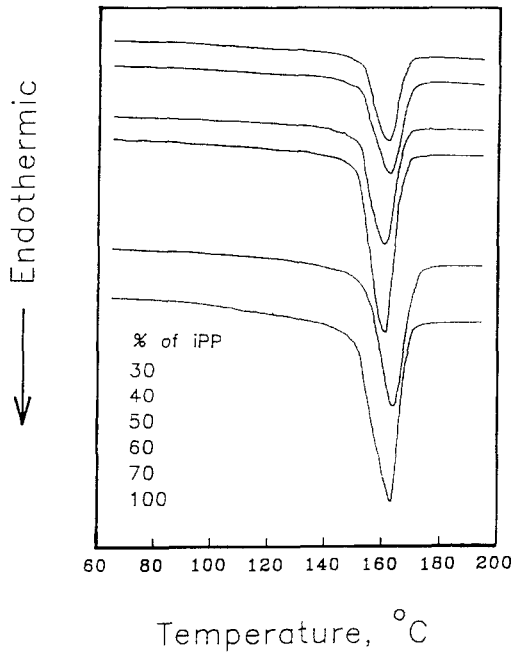

Figure 1 D.s.c. thermograms of various isotactic PP/EPDM blends

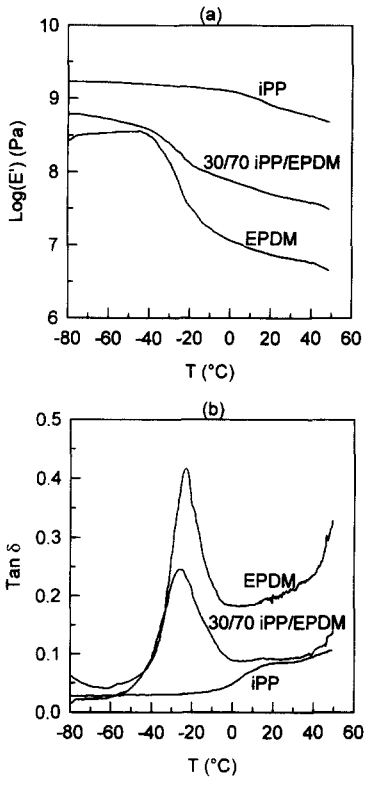

Figure 2 Temperature dependence of dynamic storage modulus and loss tangent of pure iPP, pure EPDM and the 30/70 iPP/EPDM blend

vacuum oven at 50°C for 48 h and then melt-pressed in a laboratory hot press at 200°C for 20 min at an elevated pressure. The pressure was released suddenly, and then increased again; this procedure was repeated several times to remove any trapped bubbles. The moulded films were cut into a ribbon shape of an appropriate size (50 mm length, 5 mm width and 300 μm thickness) for dynamic mechanical tests. Melting and crystallization studies were conducted on a Du Pont thermal analyser (Model 9900) coupled with a heating module (Model 910) from −100 to 200°C under nitrogen circulation. The heating rate was 10°C min^{-1}. An indium standard was used for temperature calibration.

A cloud point measurement was performed using light scattering by first melting the crystalline phase in the blends at 170°C and by rapidly cooling to 140°C. The scattered intensity at a given scattering angle (approximately 20°) was measured during the re-heating cycle from 140 to 190°C at a rate of 0.5°C min^{-1}. Time-resolved light scattering was carried out by simultaneous measurement of scattered intensity as functions of azimuthal and scattering angles (2θ) using a two-dimensional Vidicon camera interlinked with an Optical Multichannel Analyser (OMA III)[16]. A polarizing optical microscope (POM, Nikon Optiphot 2-pol) attached to a Nikon camera (FX-35DX) was used for identifying time evolution of the structure. A temperature controller (Model 2010, Omega Eng., Inc.) was used along with a sample chamber (THMS 600, Linkam) for heating the specimens in the microscopic investigations.

RESULTS AND DISCUSSION

Miscibility characterization

The solvent-cast films of iPP/EPDM blends were turbid to the naked eye, which may be attributed to phase separation of the blends and/or the presence of iPP crystals. The second differential scanning calorimetry (d.s.c.) runs after heating to 200°C in the first runs exhibit dual glass transition temperature (T_gs), but no appreciable movement of the T_g was discerned in their blends. The melting transition of the iPP shows little or no change (only a few degrees), with the addition of EPDM (*Figure 1*). The crystallization temperature also remains virtually constant with increasing EPDM content, suggesting that iPP and EPDM are immiscible below the crystallization temperature of iPP.

Dynamic mechanical experiments were carried out on the 30/70 iPP/EPDM blend. *Figure 2* exhibits temperature dependence of the storage modulus and loss tangent for the pure iPP, the pure EPDM, and their 30/70 blend. The loss tangent peaks corresponding to the glass transitions of the iPP and EPDM constituents were clearly discernible at around 10 and −28°C, respectively. The pure EPDM shows a small hump at around 10–20°C in the tan δ curve, which may be attributed to the presence of a minute amount of propylene segments in the EPDM copolymer. The 30/70 iPP/EPDM blend reveals dual loss peaks, corresponding to that of their constituents. The virtual lack of peak movement supports the above conclusion from the d.s.c. studies that the crystalline iPP/EPDM samples moulded at 200°C are phase separated. This finding is consistent with the results obtained by others for the melt-mixed conventional PP/EPDM blends[11–15].

Phase diagram determination

Figure 3 shows the variation of scattered intensity of the 50/50 iPP/EPDM blend during the course of heating at 0.5°C min^{-1}. The intensity starts to decay at the onset (140°C) of crystal melting of the iPP in the blend. This trend continues with progressive crystal melting until phase separation begins around 155°C, giving rise to an abrupt increase in intensity. This temperature is evidently well below the crystal melting temperature

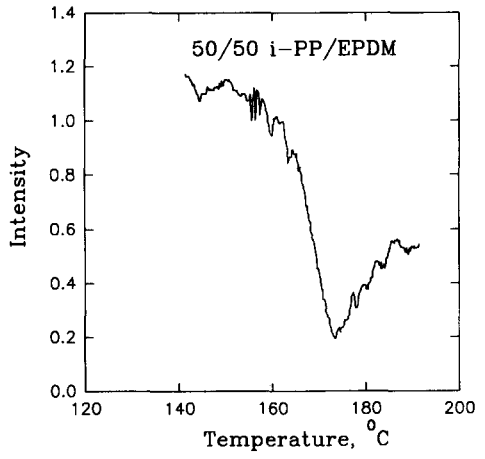

Figure 3 Variation of scattered intensity at an arbitrary scattering angle ($2\theta = 20°$) of the solvent-cast 50/50 blend. The heating rate was 0.5°C min^{-1}

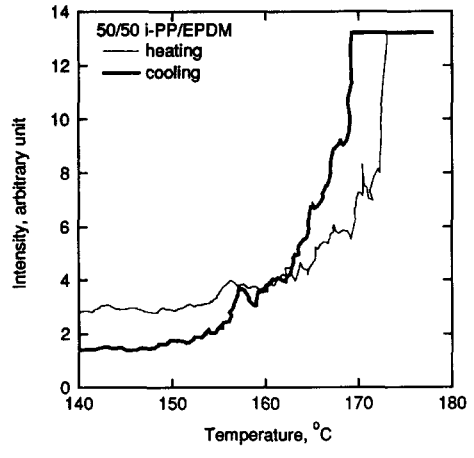

Figure 4 The second run of the 50/50 blend from 140°C at the heating rate of 0.5°C min^{-1} after melting the sample at 170°C and rapidly cooling it down to 140°C

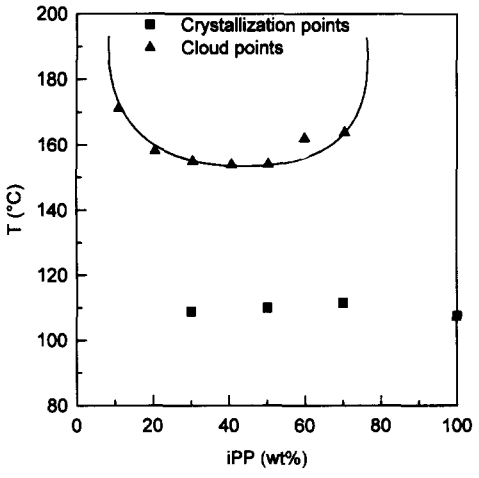

Figure 5 A cloud point phase diagram of the amorphous iPP/EPDM

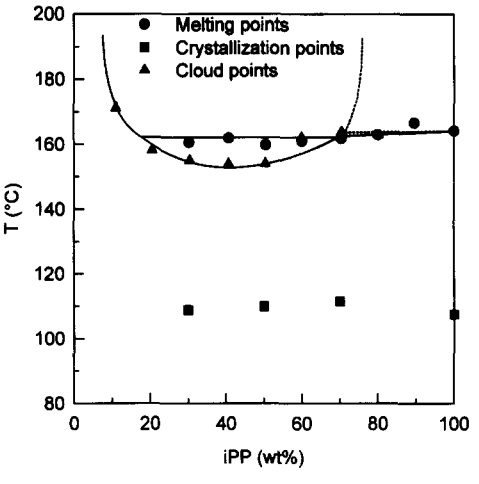

Figure 6 The coupling between the cloud point phase diagram of the iPP/EPDM and the melting transition of iPP in their blends in conjunction with the crystallization temperatures

obtained by the d.s.c. technique. This observation is not surprising, in view of the fact that iPP molecules probably have gained sufficient mobility during premelting, so that phase separation could start before the crystal melting has completed. However, the coupling between the iPP crystal melting and liquid–liquid phase separation makes the determination of the cloud point temperature extremely difficult, i.e. it is almost impossible to locate the coexistence line of the lower critical solution temperature (LCST) by the present conventional cloud point technique.

To circumvent such a problem, the 50/50 iPP/EPDM blend specimen was first heated for 2 min above the crystal melting temperature (170°C), and immediately cooled down to 140°C in 2 min. This time appeared sufficient for completing the re-mixing due to fast mutual diffusion (homogenization). Subsequently, the temperature was raised again at 0.5°C min^{-1} to mimic the phase separation temperature without the influence of crystal melting. In view of the short time interval, the blend should be practically in the melt state at 140°C. As can be seen in *Figure 4*, the scattered intensity initially remains constant, suggestive of homogeneous character of the blend in the melt state (140–150°C), but it increases abruptly as liquid–liquid phase separation commences at about 155°C. This is thermally reversible, so long as the phase separation process has not advanced significantly.

Based on this methodology, the cloud point temperatures for other compositions were determined in order to establish a temperature–composition phase diagram, which is a LCST in character (*Figure 5*).

To elucidate the coupling between crystal melting and liquid–liquid phase separation of the iPP/EPDM blends, this LCST phase diagram is depicted, together with the melting and crystallization temperatures (*Figure 6*). Recall that the melting temperatures obtained by d.s.c. at 10°C min^{-1} are by no means at equilibrium. The determination of the crystal melting at very slow heating rates will generally be influenced by the well-known annealing effect leading to crystal perfection through melting–recrystallization or lamellar thickening[17]. Hence, the equilibrium melting temperature must be higher than hitherto reported, and thus the melting transition must be coupled with the LCST. The premelting temperatures of iPP fall within the miscibility gap bounded by the crystallization temperatures and the LCST, and thus the homogenization process would occur below this liquid–liquid phase separation temperature. Nevertheless, it is reasonable to infer that the phase separation process probably starts the moment the iPP crystals begin to melt.

Another interesting feature concerning this phase diagram is the possible coexistence of iPP melt and

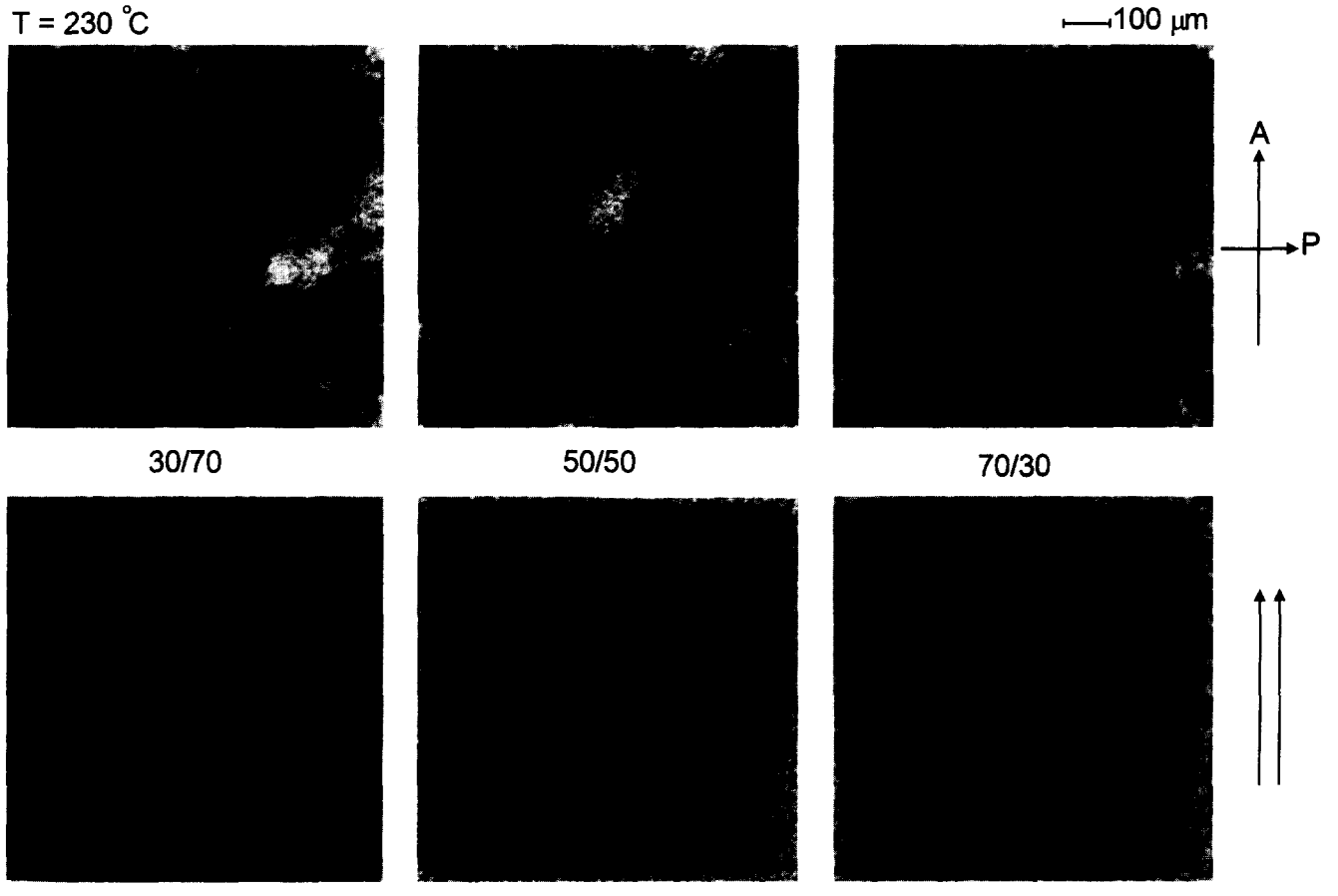

Figure 7 The overgrowth of spherulitic structures over the phase separated domains of the 30/70, 50/50, and 70/30 iPP/EPDM blends following slow cooling from 230°C to ambient temperature

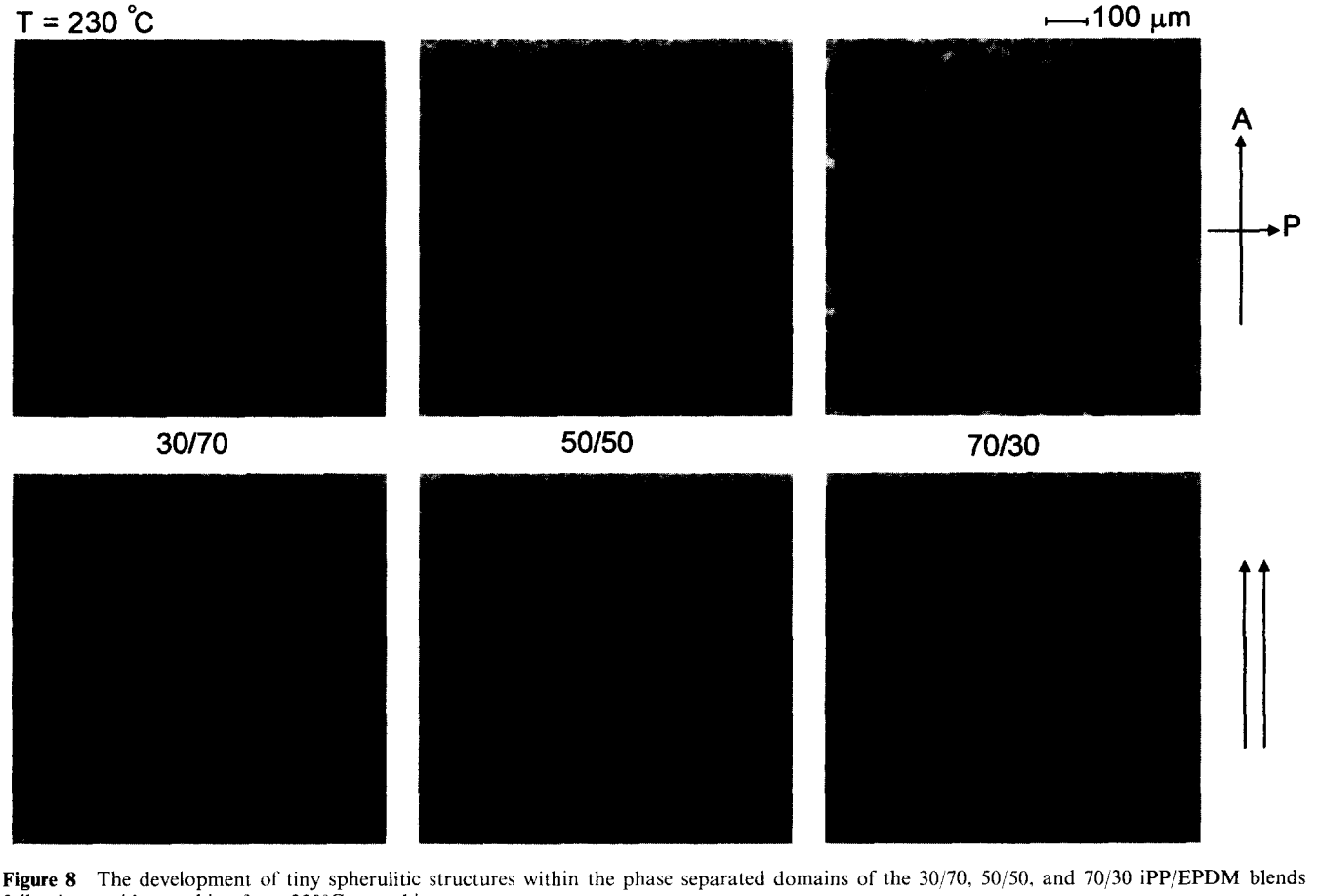

Figure 8 The development of tiny spherulitic structures within the phase separated domains of the 30/70, 50/50, and 70/30 iPP/EPDM blends following rapid quenching from 230°C to ambient temperature

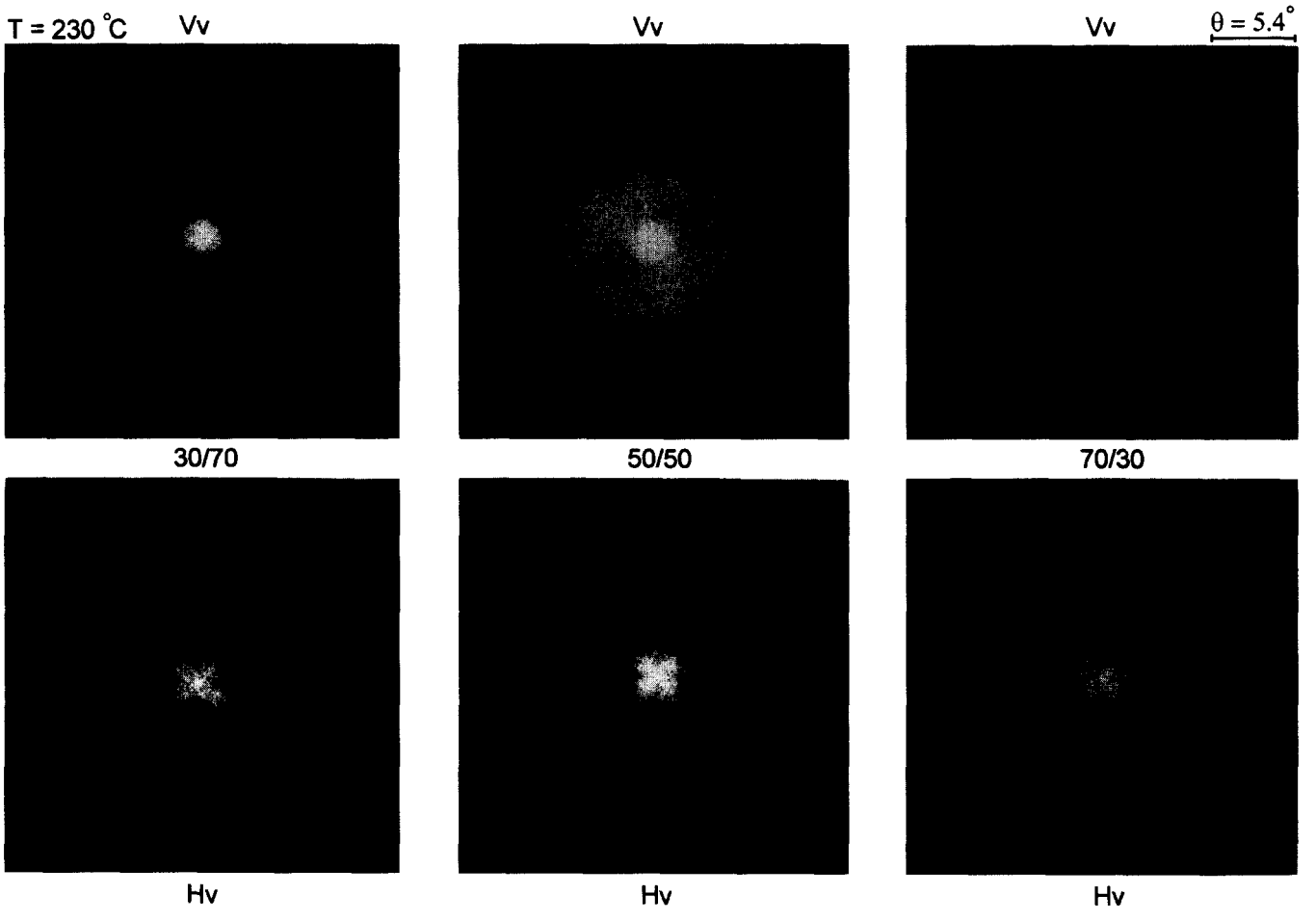

Figure 9 The light scattering patterns under Hv and Vv configurations corresponding to *Figure 7*, showing the overgrowth of the spherulitic structures over the phase separated domains during slow cooling

amorphous EPDM at some high iPP compositions. When the pure iPP crystals undergo melting, the iPP melt is always isotropic. It can be expected that the iPP-rich compositions remain in a single phase, since these blends would be outside the envelope of the LCST (shown by a hypothetical dotted line to guide the eye). A preliminary investigation on the 95/15 iPP/EPDM composition revealed a single phase at 180°C, but it showed two-phase modulated structures upon quenching to room temperature[18]. The metastable iPP melt + EPDM coexistence phase must exist in a narrow temperature gap so that the chemical potentials of the two coexistence phases may be balanced. The influence of crystal melting on the dynamics of liquid–liquid phase separation is expected to be more profound in such high iPP-rich blends, relative to that of the low iPP content mixtures; this complex non-equilibrium problem will be addressed in a future paper[18].

Crystallization and structure formation

The miscibility gap between the crystallization temperature and the LCST of the amorphous iPP (melt)/EPDM blends has probably helped in obtaining a homogeneous blend, at least in their melt state. Upon cooling, the crystallization of iPP would reject any amorphous materials such as amorphous iPP and EPDM from the crystallizing front. However, parts of the amorphous iPP chains must be attached to the crystal lattice in the forms of cilia, loops, or tie chains. Such a transition zone of the crystal surfaces may therefore be rich in amorphous iPP relative to that in the bulk where EPDM chains are expected to be rich.

Conceptually, it seems plausible that crystallization can induce not only liquid–solid phase separation between iPP crystals and amorphous iPP/EPDM, but also liquid–liquid phase separation between amorphous iPP and EPDM during the course of crystallization as mentioned above. *Figure 7* illustrates the development of spherulite formations and bicontinuous structure of the 70/30, 50/50, and 30/70 iPP/EPDM blends during the course of slow cooling (0.5°C min^{-1}). Tiny modulated structures, which are a signature of liquid–liquid phase separation by spinodal decomposition, can be discerned within the large spherulitic structures, suggesting that liquid–liquid phase separation has already occurred at the onset of crystallization. It is apparent, however, that the spherulite of iPP has overgrown the phase separated spinodal structure. If the blend specimens were quenched rapidly from the melt to ambient temperature, no distinct spherulitic structure developed during the POM investigation. These POM patterns are birefringent, but are rather reminiscent of the modulated spinodal structure (*Figure 8*). Nevertheless, a diffuse four-lobe-clover pattern can be discerned by depolarized light scattering, suggestive of the development of small and perhaps incomplete spherulitic textures. It is believed that iPP crystallization must have taken place within these modulated phase separated domains. These morphological results clearly suggest that there is a competition between the crystallization and phase separation,

probably driven by an upper critical solution temperature (UCST). Although the exact UCST coexistence line is not identifiable in the present system, due to the implication of iPP crystallization, the possible existence of a similar UCST had been demonstrated experimentally by Shimada *et al.*[19] and Tomura *et al.*[20] in a different crystal/amorphous polymer blend, viz., poly(vinylidene fluoride) (PVDF)/poly(methyl methacrylate) (PMMA). The observed two-phase structure of the iPP/EPDM is in good accord with the revelation of the dual T_gs in the dynamic mechanical studies in *Figure 2*, as well as by others[11–15]. Although the UCST may be responsible for the immiscibility of iPP/EPDM blends at ambient temperature, one cannot rule out the possibility of a frozen-in two-phase structure due to the LCST, because the present 30/70 iPP/EPDM blends for the dynamic mechanical tests were moulded at 200°C, which is above the LCST. To distinguish these two possible causes for the immiscibility of the present iPP/EPDM system, a temperature quench experiment may be important. This will be described in more detail in a future paper[18].

Figure 9 exhibits the light scattering patterns of the intermediate blends obtained by using Hv (horizontal polarizer with vertical analyzer) and Vv (both polarizers are vertical) conditions. Under the Vv conditions, that are sensitive to both concentration fluctuations and orientation fluctuations, a diffused scattering halo was discerned, similar to that observed without using any polarizers. The appearance of a Vv scattering halo indicates the dominant contribution from the concentration fluctuations (due to the large refractive index contrast between iPP and EPDM) arising from phase separation, as compared with that of crystallization. The Hv scattering, which is predominantly contributed to by the orientation fluctuations, permits us to selectively probe the crystallization process in the present system. The typical four-lobe-clover pattern appears small relative to the diameter of the scattering halo, which in turn suggests that the iPP spherulites have overgrown the phase separated domains. These light scattering results are in good agreement with the above POM investigation. It is reasonable to conclude that the ultimate morphologies are strongly dependent on the competition between the dynamics of liquid–liquid phase separation and crystallization kinetics. The subject of dynamical aspects of liquid–liquid phase separation induced by temperature jumps above the LCST and the coupling between the crystallization and phase separation driven by thermal quenching (UCST) will be of interest, and is left to the scope of a future study[18].

CONCLUSIONS

We have demonstrated that the iPP/EPDM blends are immiscible, except in a limited temperature gap bound by the crystallization temperature and the crystal melting temperature. Near the melting temperature of iPP, liquid–liquid phase separation occurred and exhibited an LCST phase diagram. Upon cooling, the crystallization of iPP probably drove the system to phase separate into iPP-rich and iPP-poor regions, suggesting a possible existence of a UCST. On the other hand, the presence of the dual T_gs in the dynamic mechanical studies of the 30/70 iPP/EPDM blend may be due to the fact that the moulding temperature of 200°C was well above the LCST. Hence, one cannot rule out the possibility that the observed immiscibility of the iPP/EPDM blends in the dynamic mechanical tests may be due to the frozen-in two phase structure from the above LCST. The morphology of the phase separated domains driven by crystallization resembled the spinodal structure, but the PP spherulites had overgrown these phase separated domains.

REFERENCES

1. Nishi, T. and Wang, T. T., *Macromolecules*, 1975, **8,** 909.
2. Olabisi, O., Robeson, L. M. and Shaw, M. T., *Polymer–Polymer Miscibility*. Academic Press, New York, 1979.
3. Cheung, Y. W. and Stein, R. S., *Macromolecules*, 1994, **27,** 2512.
4. Cheung, Y. W., Stein, R. S., Lin, J. S. and Wignall, G. D., *Macromolecules*, 1994, **27,** 2520.
5. Cham, P. M., Lee, T. H. and Marand, H., *Macromolecules*, 1994, **27,** 4263.
6. Penning, J. P. and Manley, R. St J., *Macromolecules*, 1996, **29,** 77.
7. Penning, J. P. and Manley, R. St J., *Macromolecules*, 1996, **29,** 84.
8. Fujita, K., Kyu, T. and Manley, R. St J., *Macromolecules*, 1996, **29,** 91.
9. Tanaka, H. and Nishi, T., *Phys. Rev., A*, 1989, **39,** 783.
10. Hashimoto, T., Inaba, N., Sato, K. and Suzuki, S., *Macromolecules*, 1986, **19,** 1690.
11. Coran, A. Y. and Patel, R., US Patent No. 4297453, 1981.
12. Coran, A. Y. and Patel, R., US Patent No. 4310638, 1982.
13. Coran, A. Y. and Patel, R., US Patent No. 4350470, 1982.
14. Coran, A. Y., in *Handbook of Elastomers: New Developments and Technology*, ed. A. K. Bhowmick and H. L. Stephens. Marcel Dekker, New York, 1988, p. 249.
15. Goettler, L. A., Richwine, J. R. and Wille, F., *J. Rubber Chem. Tech.*, 1982, **55,** 1558.
16. Kyu, T. and Saldanha, J. M., *J. Polym. Sci., Polym. Lett. Edn.*, 1988, **26,** 33.
17. Geil, P. H., *Polymer Single Crystals*. Krieger, Huntington, NY, 1973.
18. Kyu, T., Chen, C. Y. and Ramanujam, A., unpublished work.
19. Shimada, S., Hori, Y. and Kashiwabara, H., *Macromolecules*, 1988, **21,** 3454.
20. Tomura, H., Saito, H. and Inoue, T., *Macromolecules*, 1992, **25,** 1611.